

Ultra-bright and efficient single photon generation based on N-V centres in nanodiamonds on a solid immersion lens

Tim Schröder, Friedemann Gädeke, Moritz Julian Banholzer and Oliver Benson

Humboldt-Universität zu Berlin
Institut für Physik, AG Nano Optics
Newtonstr. 15, 12489 Berlin

E-mail: tim.schroeder@physik.hu-berlin.de

Abstract. Single photons are fundamental elements for quantum information technologies such as quantum cryptography, quantum information storage and optical quantum computing. Colour centres in diamond have proven to be stable single photon sources and thus essential components for reliable and integrated quantum information technology. A key requirement for such applications is a large photon flux and a high efficiency. Paying tribute to various attempts to maximise the single photon flux we show that collection efficiencies of photons from colour centres can be increased with a rather simple experimental setup. To do so we spin-coated nanodiamonds containing single nitrogen-vacancy colour centres on the flat surface of a ZrO_2 solid immersion lens. We found stable single photon count rates of up to 853 kcts/s at saturation under continuous wave excitation while having excess to more than 100 defect centres with count rates from 400 kcts/s to 500 kcts/s. For a blinking defect centre we found count rates up to 2.4 Mcts/s for time intervals of several ten seconds. It seems to be a general feature that very high rates are accompanied by a blinking behaviour. The overall collection efficiency of our setup of up to 4.2% is the highest yet reported for N-V defect centres in diamond. Under pulsed excitation of a stable emitter of 10 MHz, 2.2% of all pulses caused a click on the detector adding to 221 kcts/s thus opening the way towards diamond based on-demand single photon sources for quantum applications.

Increased single photon collection with high on-demand efficiency allows for higher communication bit rates in quantum cryptography [1] and faster read out of stationary qubits [2, 3]. Also, a key operation in quantum information processing (QIP), i.e. two-photon interference, requires a large photon flux. Advanced protocols, such as entanglement swapping or entanglement transfer [4, 5] also won't be possible if photons as flying qubits cannot be generated or collected efficiently. A first crucial step concerns reliable single photon generators. Such systems have been realised based on atoms [6, 7], ions [8], molecules [9], and solid state based emitters like quantum dots [10] or defect centres in diamond [11]. There were also successful attempts to integrate solid-state emitters in photonic nano-structures to increase the photon flux [12, 13, 14]. In particular defect centres in diamond have drawn a lot of attention lately as they are photostable even at room temperature. Since the first prove that single photons can be collected from nitrogen-vacancy defect centres in diamond more than ten years ago [11], steady improvement of collection rates has been achieved. Furthermore other defect centres with different optical behaviour have been found and fabricated [15, 16, 17] in bulk as well as in diamond nanocrystals. Nanodiamonds have several advantages compared to bulk diamond as they can be easily deposited on various substrates with e.g. spin-coating techniques or nano-manipulation. AFM manipulation has been used to integrate them on photonic crystal resonators [18] or on optical fibres [19]. Moreover photon collection efficiency of nanodiamonds is generally higher [20]. Yet it has just recently been shown, that reduction of excitation intensity and improvement of emission collection of N-V centres in bulk diamond can be achieved via etching adequate structures into CVD grown bulk diamond [21, 22, 23]. These structures can be nanorods [21] or solid immersion lenses built into bulk diamond [22] or made out of bulk diamond [23] and facilitate collection of single photons of up to 500 kcts/s. Unfortunately production of these structures demands rather sophisticated processes.

Solid immersion lenses (SIL) on the other hand have been integrated into optical microscopes 1990 [24] and are commercially available in various designs. A solid immersion lens can be formed as a simple half-sphere or in a so called Weierstrass-design [25] and is most typically made of high index material, e.g. ZrO_2 with $n = 2.17$. The operation principle of a SIL is very similar to an oil-immersion microscope. Samples are either deposited on or close to the flat side of the SIL while the optical access lies on the curved side of the SIL. In this manner the wave front of a focused light beam passes the surface parallel and neither refraction nor aberration is taking place. Due to the high index of refraction the numerical aperture is enhanced warranting higher collection angles and thus higher emitter collection rates. Also the resolution is increased similar as in oil-immersion-microscopes and much higher energy densities in the focus are obtained [24]. With respect to the implementation of SILs with a single photon emitter there is another important feature. On account of the strong step in the index of refraction at the SIL-air interface the dipole emission is not symmetrically distributed into SIL and air respectively [26]. We performed finite difference time domain (FDTD) calculations for our specific system and found that a simple dipole emitter in air, 10 nm

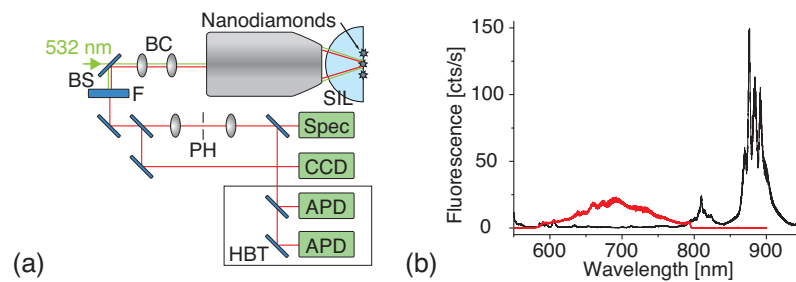


Figure 1. Experimental setup and spectroscopic properties of the solid immersion lens. (a) Sketch of home-built confocal microscope. BC, BS, F, PH, HBT stand for beam control, beam splitter, filter, pinhole, Hanbury Brown and Twiss setup, respectively. (b) Spectrum of the solid immersion lens fluorescence (black curve) at excitation power of $933 \mu\text{W}$ and spectrum of N-V centre on SIL, emission cut off by 590 nm long pass and 795 nm short pass filters (red curve).

away from a flat material surface with $n = 2.17$, emits more than 86 % of its emission into the direction of the SIL if oriented parallel to the surface and more than 75 % if oriented perpendicular to the surface. These results are in agreement with an analytical analysis of a dipole emitter in front of a flat dielectric interface [27]. The combination of commercial availability, easy experimental integration, well increased NA, smaller focus and strongly enhanced emission into direction of collection, make a solid immersion lens a very potent tool to increase single photon emitter collection efficiencies.

Here we present the experimental implementation of a SIL microscope combined with the advantages of nanodiamonds which outperform so-far reported single photon count rates from N-V centres in diamond. By spin-coating nanodiamonds on the flat surface of commercially available ZrO_2 half-spheres we prepared a SIL suitable to efficiently excite colour centres inside the nanodiamonds. The SIL was implemented into a home-built confocal microscope featuring an air objective with a numerical aperture of 0.9 and a pinhole of $100 \mu\text{m}$ as depicted in figure 1(a). To reduce stray light from laser excitation and SIL fluorescence 540 nm and 590 nm long pass filters as well as a 795 nm short pass filter were used. Via the spin-coating technique there is a wide flexibility to integrate nanodiamonds with arbitrary colour centres into any kind of SIL. The latter can be half-sphere SILs or Weierstrass SILs made of various materials transparent at excitation and colour centre emission wavelength. The chosen material ZrO_2 has a high index of refraction n of 2.17 at 600 nm and can be processed by diverse companies to half-spheres within required tolerances [28]. Its intrinsic fluorescence due to impurities is sufficiently negligible between wavelengths of 615 nm and 785 nm at typical excitation powers for defect centres in diamond of less than 1 mW (see spectrum in figure 1(b)). It is well suitable for the collection of photons from e.g. N-V centres [11], Ni/Si related centres [29, 30] and Si-V centres [16, 31] emitting from 600 nm to 800 nm (see spectrum of a N-V centre in figure 1(b)), around 770 nm and around 740 nm, respectively.

For the applied spin-coating process an aqueous solution with 0.01 % polyvinyl alcohol and nanodiamonds with a mean size of 25 nm was prepared. Spin-coating of

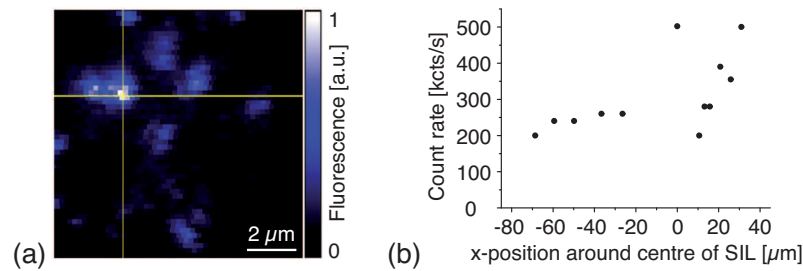


Figure 2. x-y-confocal scan of nanodiamond emission on SIL and distribution of N-V centre intensity. (a) 10 μm by 10 μm intensity scan of an area close to the centre of the SIL. Such area scans most likely feature a couple bright ($R_{\text{Inf}} = 400$ kcts/s to 700 kcts/s) and many darker N-V centres ($R_{\text{Inf}} < 400$ kcts/s). (b) Count rate of different N-V centres under pulsed excitation of 80 MHz and excitation intensities of 148 μW in the focus. 12 N-V centres along one scan direction (x-axis) were investigated. All emitters provide single emitter characteristics proven by a measured value of the normalized 2nd order correlation function $g^{(2)}(0) < 0.5$.

a solution with suitable diamond density was performed with 2000 rpm to ensure a dense distribution of the diamonds with distances smaller 1 μm . Figure 2(a) shows a x-y-intensity scan of the confocal microscope of a 10 μm x 10 μm region with typical diamond distribution and fluorescence intensity. We found that in a rectangular array of about 10 μm by 100 μm around the centre of the SIL at least 10 diamonds have count rates of more than 250 kcts/s if excited with 148 μW of quasi-CW excitation with laser repetition rate of 80 MHz while many more had count rates around 200 kcts/s (see figure 2(b)). It should be mentioned that many of the diamonds investigated showed blinking behaviour. Comparing these count rates to saturation measurements (see e.g. figure 3(a)) we extrapolate count rates at saturation under CW excitation of 400 kcts/s to 500 kcts/s for the 10 measured defect centres. For an area of 100 μm by 100 μm we expect more than 100 colour centres with similar emission rates. In this manner suitable diamonds for special applications can be selected, e.g. one diamond with maximum collection rates or two diamonds with matching zero phonon line emission for two-photon interference experiments.

To prove single photon character of studied colour centre emissions we performed autocorrelation measurements in a Hanbury Brown and Twiss (HBT) setup (see figure 1(a)). If the normalized intensity autocorrelation function

$$g^{(2)}(\tau) = \frac{\langle I(t) I(t + \tau) \rangle}{\langle I(t) \rangle^2}$$

has values at zero time delay $\tau = 0$ of $g^{(2)}(0) < 0.5$, emission should occur basically from a single N-V centre. Typical $g^{(2)}(\tau)$ functions of the measured N-V centres have a $g^{(2)}(0)$ between 0.1 and 0.3, depending on excitation intensities. In order to determine the maximum accessible photon flux we performed saturation measurements (displayed

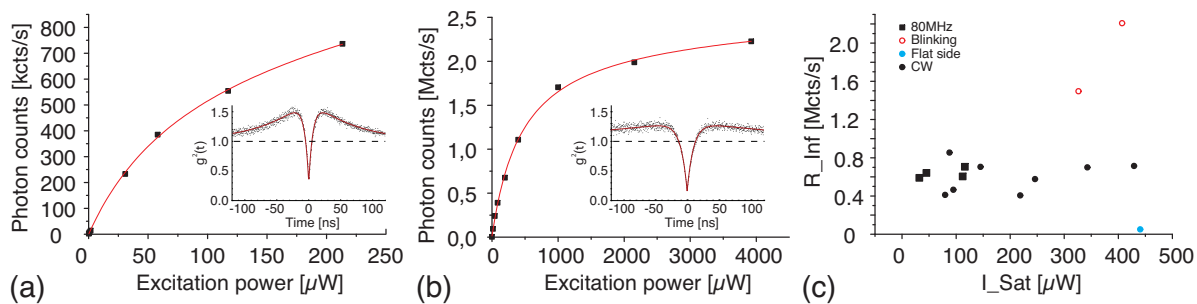


Figure 3. Autocorrelation and saturation measurements of different N-V centres. (a) Saturation measurement of the brightest stable emitter found. R_{Inf} is 853 kcts/s while saturation excitation intensity is $88 \mu\text{W}$. The inset shows the normalised autocorrelation function $g^{(2)}(\tau)$ of the same emitter with $g^{(2)}(0) < 0.3$. (b) Saturation measurement of the brightest blinking emitter found. R_{Inf} is 2.4 Mcts/s on a time basis of several ten seconds while saturation excitation intensity is $464 \mu\text{W}$. The averaged count rate is 477 kcts/s for an excitation intensity of 2.6 mW. The inset shows the normalised autocorrelation function $g^{(2)}(\tau)$ of the same emitter with $g^{(2)}(0) < 0.16$ at excitation of 1 mW. The red curves in (a) and (b) are theoretical fits to the data (see text). (c) Saturation count rates of different N-V centres as function of saturation excitation intensities. Black symbols represent stable emitters, open red circles blinking ones and the blue dot represents a N-V centre probed from the flat side of the SIL (the right side of the SIL in figure 1(a)). Square symbols denote quasi-CW excitation with 80 MHz laser repetition rate while circles relate to CW excitation.

in figure 3(a),(b)). Fits to the experimental curves were done according to

$$R(I) = \frac{R_{\text{Inf}} I}{I_{\text{Sat}} + I} + (A + \alpha)I + \beta$$

where R is the single photon count rate, R_{Inf} the count rate at infinite excitation intensities, I the excitation intensity, I_{Sat} the saturation excitation intensity, A represents the measured background fluorescence $1 \mu\text{m}$ away from the N-V centre, while α and β are fit parameters for linear background stemming from the diamond and additional background such as APD dark counts and residual stray light, respectively. Most saturation excitation intensities were distributed around $80 \mu\text{W}$ in the focus while the typical single photon count rate R was 500 kcts/s without background subtraction as can be seen in figure 3(c). Twelve single N-V centres of similar brightness were analyzed. It should be pointed out though that these N-V centres have quite different saturation intensities as can be derived from figure 3(c). This is to some degree due to their randomly distributed dipole orientations. Furthermore the nanodiamonds have mismatched physical and optical contact to the SIL surface resulting in diverse optical coupling of the nanodiamonds to the SIL. In figure 3(c) also the count rate at saturation for a random N-V centre that has been probed from the air side of the SIL is depicted. This N-V centre, the brightest we found from the flat side, shows count rates at saturation of 50 kcts/s, about ten times lower intensity than those excited through the SIL. Furthermore its saturation intensity of $440 \mu\text{W}$ is also about 5 times higher compared to these N-V centres.

We found one outstanding N-V centre with a stable single photon count rate at saturation of 853 kcts/s. Even at excitation intensities of $213 \mu\text{W}$ and count rates of 736 kcts/s its $g^{(2)}(0)$ value was smaller than 0.3 and could be further reduced by adequate filtering (see figure 1(b)). Furthermore we observed another remarkable single defect centre. This defect centre was ultra bright as we found single photon rates up to 2.4 Mcts/s at saturation on a time base up to several ten seconds alternating with darker periods. On the average, the single photon emission rate was 400 kcts/s at excitation power of 2.6 mW. We also measured its autocorrelation function at count rates of up to 1.1 Mcts/s to be smaller than $g^{(2)}(0) < 0.16$. In our experiments we found that in an ensemble of nanodiamonds there exist a few ultra-bright N-V defect centres with rates > 1 Mcts/s. However, this large rate seems to be accompanied by pronounced blinking behaviour. The reason for this is not yet understood.

For most applications of single photons in QIP an on-demand generation is required [32]. One possibility is to use pulsed excitation. A crucial parameter of such a source is the collection efficiency per excitation pulse. A perfect single photon on-demand device would deliver exactly one detected single photon per pulse in a well defined optical mode. Such performance is limited in real devices mainly by the efficiency to collect single photon emission with the first lens, losses in the optical pass towards the detector as well as by detector efficiencies.

To determine the collection efficiency of our setup we measured the collection efficiency per excitation pulse. The repetition rate of the pulsed excitation laser was limited to about 10 MHz, such that the time interval between pulses was 100 ns, i.e. much larger than the lifetime of 18 ns of the N-V centre. With these numbers the probability for excited N-V centres to decay before the arrival of the next exciting pulse was 0.97. If we further assume that the excitation probability is one, which is justifiable because we performed the experiments at saturation, we can directly deduce the collection efficiency of the setup from the measured count rate. We reached a stable collection efficiency of $\eta = 2.7\%$ in saturation, estimated from experimental collection efficiency at 10 MHz laser rate, while having a total single photon count rate of 267 kcts/s in saturation (see figure 4(b),(c)).

A more detailed analysis can be based on a two-level model. This simple model describes the measured count rate $r(\Gamma)$ of the laser repetition rate Γ . Assuming an excitation probability of one which is justifiable as explained above, only the collection efficiency η , the lifetime of the emitter γ^{-1} and the laser repetition rate Γ influence the single photon count rate

$$r(\Gamma) = \eta \cdot \Gamma \cdot \gamma \cdot \int_0^{1/\Gamma} e^{-\gamma t} dt = \eta \cdot \Gamma \cdot (1 - e^{-\gamma/\Gamma}).$$

We used this model for the fit in figure 4(c) where the count rate in saturation is displayed as a function of the laser rate. From the fit the photon collection efficiency η can be deducted. A value of $\eta = 2.6\%$ for the total collection efficiency is found in

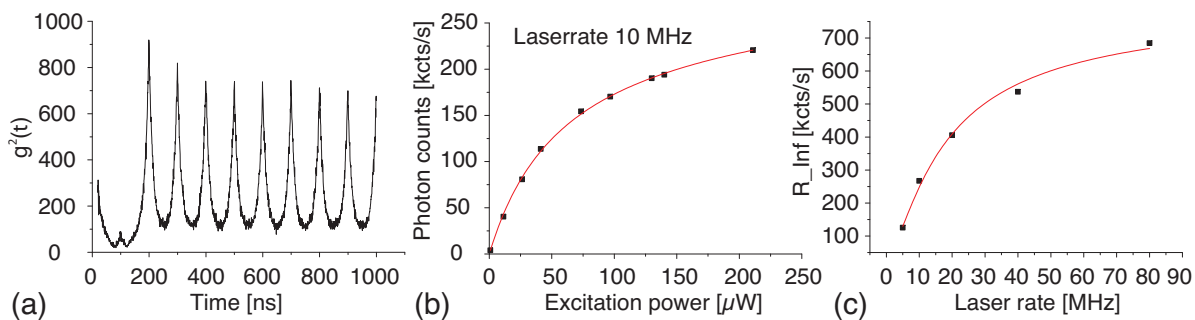


Figure 4. Pulsed autocorrelation function, saturation measurement at pulsed excitation, and emission in saturation as function of laser rate. (a) Pulsed autocorrelation measurement with $g^{(2)}(0) = 0.16$ of the stable, bright emitter depicted in figure ?? excited at excitation intensity of $77 \mu\text{W}$ with 10 MHz laser rate and count rates of 221 kcts/s. (b) Saturation curve of the same emitter as in (a) under pulsed excitation of 10 MHz with $R_{\text{Inf}} = 267$ kcts/s and $I_{\text{Sat}} = 60 \mu\text{W}$. The red curve is a theoretical fit to the data (see text). (c) R_{Inf} as function of laser repetition rate. The theoretical fit to the data (red curve) is further explained in the text.

agreement with the estimated η of 2.7%. This is the highest yet reported collection efficiency for a stable N-V defect centre in diamond. Furthermore collection efficiency for the blinking defect centre with count rates up to 2.4 Mcts/s at CW excitation (see figure 3(b)) was even higher. It also emits ultra-high single photon flux when excited with pulsed laser light. At laser repetition rates of 10 MHz and $385 \mu\text{W}$ up to 420 kcts/s were detected. This determines a collection efficiency of 4.2% on a timescale of several ten seconds. The determined setup efficiency η_{Setup} after the flat surface of the SIL of $\eta_{\text{Setup}} < 0.23$ gives a source efficiency ϵ , i.e. fraction of light collected by the first objective, of $\epsilon > 11.7\%$ and $\epsilon > 18.3\%$ for the stable and the blinking defect centre respectively. η_{Setup} was calculated from reflection and transmission parameters of all optical elements according to their data sheet values.

Single photon emission character of the emitters excited with pulsed laser light was also proven measuring the normalized intensity autocorrelation function $g^{(2)}(\tau)$. Figure 4(a) depicts the pulsed autocorrelation function of the N-V centre with $g^{(2)}(0) = 0.16$ at excitation intensity of $77 \mu\text{W}$ and count rates of 221 kcts/s. Emission under pulsed excitation generally provides a better suppression of background photons compared to CW excitation as excitation radiation is limited to periods when the electron is in the ground state, i.e. can be excited and emit a single photon. The bright blinking defect centre had $g^{(2)}(0) = 0.11$ while excited with laser rates of 10 MHz and $385 \mu\text{W}$ excitation power.

In conclusion, we report on an experimentally simple, but efficient way to strongly enhance collection of single photons emitted by N-V centres in diamond at room temperature. We integrated a ZrO_2 solid immersion lens with spin-coated nanodiamonds on its flat surface into our confocal microscope. We measured count rates in saturation

of up to 853 kcts/s for a stable N-V centre and up to 2.4 Mcts/s for a blinking defect centre. Furthermore, our compact SIL design provides access to about 100 N-V centres that emit more than 400 kcts/s. The overall collection efficiency of our setup is up to 4.2% while having a source efficiency ϵ of up to $\epsilon > 18.3\%$, opening the way towards much more efficient diamond based on-demand single photon sources. Furthermore the setup is so versatile that any kind of defect centre located in a nanodiamond can be implemented thus allowing to integrate even brighter emitters with smaller bandwidth. For a single Si-V centre with a lifetime of 1.2 ns as was just very recently presented [31] we would expect count rates up to 10 Mcts/s. Also cryogenic experiments will be possible as the immersion microscope works oil free leading off towards two-photon interference experiments.

Acknowledgement

We thank T. Aichele for fruitful discussions. Financial support of the BMBF (KEPHOSI) is acknowledged.

References

- [1] O'Brien J L, Furusawa A and Vuckovic J 2009 Photonic quantum technologies *Nat. Photon.* 3 687–95
- [2] Neumann P, Beck J, Steiner M, Rempp F, Fedder H, Hemmer P R, Wrachtrup J and Jelezko F 2010 Single-Shot Readout of a Single Nuclear Spin *Science* 329 542–4
- [3] Dutt M V G, Childress L, Jiang L, Togan E, Maze J, Jelezko F, Zibrov A S, Hemmer P R and Lukin M D 2007 Quantum register based on individual electronic and nuclear spin qubits in diamond *Science* 316 1312–6
- [4] Bouwmeester D, Pan J W, Mattle K, Eibl M, Weinfurter H and Zeilinger A 1997 Experimental quantum teleportation *Nature* 390 575–9
- [5] Schmid C, Kiesel N, Weber U K, Ursin R, Zeilinger A and Weinfurter H 2009 Quantum teleportation and entanglement swapping with linear optics logic gates *New J. Phys.* 11 033008
- [6] Kuhn A, Hennrich M and Rempe G 2002 Deterministic single-photon source for distributed quantum networking *Phys. Rev. Lett.* 89 067901
- [7] Darquie B, Jones M P A, Dingjan J, Beugnon J, Bergamini S, Sortais Y, Messin G, Browaeys A and Grangier P 2005 Controlled single-photon emission from a single trapped two-level atom *Science* 309 454–6
- [8] Keller M, Lange B, Hayasaka K, Lange W and Walther H 2004 Continuous generation of single photons with controlled waveform in an ion-trap cavity system *Nature* 431 1075–8
- [9] Lounis B and Moerner W E 2000 Single photons on demand from a single molecule at room temperature *Nature* 407 491–3
- [10] Michler P, Kiraz A, Becher C, Schoenfeld W V, Petroff P M, Zhang L, Hu E and Imamoglu A 2000 A quantum dot single-photon turnstile device *Science* 290 2282–5
- [11] Kurtsiefer C, Mayer S, Zarda P and Weinfurter H 2000 Stable solid-state source of single photons *Phys. Rev. Lett.* 85 290–3
- [12] Barnes W, Björk G, Grard J, Jonsson P, Wasey J, Worthing P and Zwiller V 2002 Solid-state single photon sources: light collection strategies *EPJD* 18 197–210
- [13] Claudon J, Bleuse J, Malik N S, Bazin M, Jaffrennou P, Gregersen N, Sauvan C, Lalanne P and Gerard J M 2010 A highly efficient single-photon source based on a quantum dot in a photonic nanowire *Nat. Photon.* 4 174–7

- [14] Dousse A, Suffczynski J, Beveratos A, Krebs O, Lemaitre A, Sagnes I, Bloch J, Voisin P and Senellart P 2010 Ultrabright source of entangled photon pairs *Nature* 466 217–20
- [15] Simpson D A, Ampem-Lassen E, Gibson B C, Trpkovski S, Hossain F M, Huntington S T, Greentree A D, Hollenberg L C L and Prawer S 2009 A highly efficient two level diamond based single photon source *Appl. Phys. Lett.* 94 203107
- [16] Wang C, Kurtsiefer C, Weinfurter H and Burchard B 2006 Single photon emission from SiV centres in diamond produced by ion implantation *J. Phys. B* 39 37
- [17] Rabeau J R, Huntington S T, Greentree A D and Prawer S 2005 Diamond chemical-vapor deposition on optical fibers for fluorescence waveguiding *Appl. Phys. Lett.* 86 134104
- [18] Wolters J, Schell A W, Kewes G, Nüsse N, Schoengen M, Doscher H, Hannappel T, Lochel B, Barth M and Benson O 2010 Enhancement of the zero phonon line emission from a single nitrogen vacancy center in a nanodiamond via coupling to a photonic crystal cavity *Appl. Phys. Lett.* 97 141108
- [19] Schröder T, Schell A W, Kewes G, Aichele T and Benson O Fiber-integrated diamond based single photon source *Nano Lett.* under reviewing process
- [20] Beveratos A, Kühn S, Brouri R, Gacoin T, Poizat J P and Grangier P 2002 Room temperature stable single-photon source *EPJD* 18 191–6
- [21] Babinec T M, M H J, Khan M, Zhang Y, Maze J R, Hemmer P R and Loncar M 2010 A diamond nanowire single-photon source *Nat. Nanotechnol.* 5 195–9
- [22] Hadden J P, Harrison J P, Stanley-Clarke A C, Marseglia L, Ho Y L D, Patton B R, O'Brien J L and Rarity J G Strongly enhanced photon collection from diamond defect centres under micro-fabricated integrated solid immersion lenses *arXiv:1006.2093v2*
- [23] Siyushev P, Kaiser F, Jacques V, Gerhardt I, Bischof S, Fedder H, Dodson J, Markham M, Twitchen D, Jelezko F and Wrachtrup J Integrated diamond optics for single photon detection *arXiv:1009.0607v1*
- [24] Mansfield S M and Kino G S 1990 Solid immersion microscope *Appl. Phys. Lett.* 57 2615–6
- [25] Terris B D, Mamin H J, Rugar D, Studenmund W R and Kino G S 1994 Near-field optical data storage using a solid immersion lens *Appl. Phys. Lett.* 65 388–90
- [26] Koyama K, Yoshita M, Baba M, Suemoto T and Akiyama H 1999 High collection efficiency in fluorescence microscopy with a solid immersion lens *Appl. Phys. Lett.* 75 1667–9
- [27] Lukosz W and Kunz R E 1977 Light emission by magnetic and electric dipoles close to a plane interface. I. Total radiated power *J. Opt. Soc. Am.* 67 1607–15
- [28] Baba M, Sasaki T, Yoshita M and Akiyama H 1999 Aberrations and allowances for errors in a hemisphere solid immersion lens for submicron-resolution photoluminescence microscopy *J. Appl. Phys.* 85 6923–25
- [29] Aharonovich I, Zhou C, Stacey A, Orwa J, Castelletto S, Simpson D, Greentree A D, Treussart F, Roch J F and Prawer S 2009 Enhanced single-photon emission in the near infrared from a diamond color center *Phys. Rev. B* 79 235316
- [30] Steinmetz D, Neu E, Meijer J, Bolse W and Becher C Single photon emitters based on Ni/Si related defects in single crystalline diamond *arXiv:1007.0202v3*
- [31] Neu E, Steinmetz D, Riedrich-Moeller J, Gsell S, Fischer M, Schreck M and Becher C Single photon emission from silicon-vacancy centres in CVD-nano-diamonds on iridium *arXiv:1008.4736v1*
- [32] Ladd T D, Jelezko F, Laflamme R, Nakamura Y, Monroe C and O'Brien J L 2010 Quantum computers *Nature* 464 45–53